AIAA JOURNAL
Vol. 30, No. 11, November 1992

Aeroacoustic Environment of an Advanced Short Takeoff and Vertical Landing Aircraft in Hover

Richard W. Wlezien*
McDonnell Douglas Research Laboratories, St. Louis, Missouri 63166
and
Peter J. Ferraro†
McDonnell Aircraft Company, St. Louis, Missouri 63166

The near-field aeroacoustic environment of a 6.02%-scale advanced short takeoff and vertical landing aircraft is investigated in proximity to a simulated ground plane. The screech and impingement-tone characteristics of twin supersonic round and rectangular plumes are shown to be highly dependent on nozzle geometry and height above the ground plane. Shadowgraph and laser-sheet flow visualization are used to clarify the flowfield mechanisms responsible for time-dependent loads due to screech, impingement tones, and unsteady impingement of the upwash on the fuselage undersurface. Detailed dynamic pressure measurements from an array of transducers on the fuselage confirm that fountain impingement is responsible for the greatest unsteady loading. Under certain conditions, high screech amplitudes produce increased dynamic loads over a large area of the fuselage and wing undersurfaces.

Introduction

THE unsteady thermoacoustic environment of a short takeoff and vertical landing (STOVL) aircraft in hover is a first-order consideration in terms of structure fatigue life and airframe weight penalties. The hover environment is highly three dimensional, unsteady, and difficult to model by other than empirical methods,[1] particularly in the case of supersonic lift jets.

Three different mechanisms can contribute to the near-field acoustic environment of the STOVL aircraft in hover. The first is the resonant interaction between the jet shear-layer instability and the shocks in a supersonic jet; this resonance is commonly known as screech. A complex interaction (screech coupling) can occur when two supersonic jets interact in a phase-locked resonance. In a series of recent papers, Seiner et al.[2,3] have shown that screech coupling can produce significant fatigue loads on surrounding aircraft structure. The second source of dynamic loading is the impingement tone,[4-6] which is a resonant interaction between the jet and the ground plane. For an aircraft in hover, impingement tones can often have significantly higher amplitudes than screech. The third source, which is unique to multiple jet impingement configurations (Fig. 1), occurs when the upwash fountain impinges on the fuselage undersurface[7-10] and generates dynamic loads by direct hydrodynamic interaction with the fuselage undersurface.

The objective of this study is to identify the dominant mechanisms responsible for aircraft dynamic loads for a STOVL aircraft in hover. The high sensitivity of jet acoustics to nozzle configuration[11-14] suggests that dynamic load minimization may be achieved by a judicious choice of nozzle shape and location. In this paper, the effects of aircraft and nozzle geometry are explored, and typical acoustic and hydrodynamic load distributions are measured on the fuselage and wing undersurfaces.

Presented as Paper 90-4016 at the AIAA 13th Aeroacoustics Conference, Tallahassee, FL, Oct. 22-24, 1990; received Jan. 28, 1991; revision received May 6, 1992; accepted for publication May 6, 1992.

*Currently Senior Scientist, High Technology Corporation, NASA Langley Research Center, Hampton, VA 23665. Associate Fellow AIAA.
†Engineer. Member AIAA.

Experimental Configuration

A primary consideration in acquiring data relevant to an advanced STOVL aircraft is the development of a model based on a viable STOVL configuration. McDonnell Aircraft Company (MCAIR) has previously designed and tested a 6.02%-scale conceptual vectored thrust configuration in proximity to a simulated ground plane in the MCAIR Jet Interaction Test Apparatus (JITA) facility. The existing model was instrumented, and acoustic loading measurements were performed in the same facility.

The model (Fig. 2) is designed for parametric variation of the aircraft configuration. It has a contoured fuselage undersurface, removable wings and tail surfaces, a flexible flow system to simulate a variety of nozzle configurations, and nozzles with a variety of exit cross sections.

The lift-nozzle arrangement used for the present study consisted of two lift jets positioned symmetrically about the aircraft centerline. Air is supplied to the nozzle system through a computer-controlled digital valve system to provide a stable nozzle pressure ratio (NPR). Both nozzles are connected to a common plenum through a symmetric flow splitter to produce equal mass flow rates through both nozzles. A provision for water injection through an orifice in the plenum is included for laser-sheet flow visualization. The water is pressurized by a booster pump system to provide continuous flow visualization capability over a wide range of operating conditions.

Four nozzle configurations were investigated with two exit shapes (round and 2:1 rectangular) and two axial variations of cross-sectional area [convergent/divergent (CD) and constant-area choked tubes (CT)]. The choice of nozzle shape was dictated by two considerations. Round plumes tend to undergo helical oscillation, whereas rectangular plumes have a

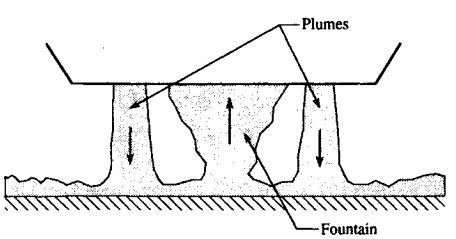

Fig. 1 Schematic of twin-plume impingement flowfield.

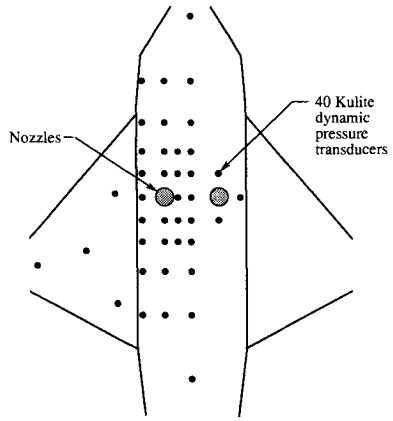

Fig. 2 Advanced STOVL configuration showing nozzles and dynamic pressure transducer locations.

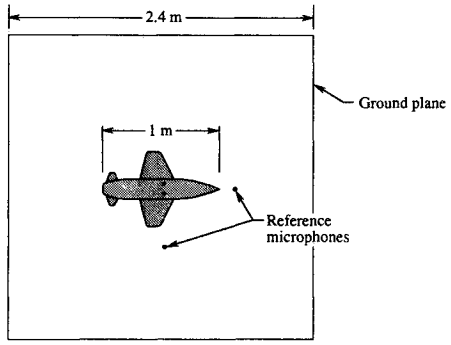

Fig. 3 Configuration for near-field acoustic measurements.

preferred screech orientation normal to the major axis of the nozzles. The CT nozzles were chosen to produce maximum screech amplitude, and the CD nozzles were chosen to minimize screech at the design pressure ratio of 3.5.

All of the nozzles have nearly identical throat areas (equivalent to a $d = 25$-mm round nozzle) to provide approximately equal mass flow through the nozzles at a given pressure ratio. The normalized nozzle center-to-center spacing, s/d, was 4.15 (104 mm) for all measurements, which was fixed by clearance holes in the model fuselage.

The nozzle exit shapes are similar for both the CD and CT nozzles, with 3.2-mm-radius fillets in the internal corners of the 2:1 rectangular nozzles. The rectangular CD nozzles contract and diverge along their minor axis only, with flat, parallel sidewalls. The subsonic section of the contractions was designed using a fifth-order polynomial having zero slope at the inlet and outlet. The supersonic section downstream of the throat was designed using an inviscid method-of-characteristics code. The nozzles were designed to have equal throat area, identical length, continuous slope and curvature at the throat, and uniform exit flow. The design Mach number of the CD nozzles is 1.47.

The ground plane (Fig. 3) is a 2.4-m square fiberglass section mounted vertically in the test cell. Variation of aircraft height above the ground is simulated by traversing the ground plane relative to the fixed model. The distance between the nozzle exit plane and the ground plane, h_n, is typically normalized with the effective nozzle diameter, d_e. The parameter d_e is the diameter of an equivalent round nozzle having a throat area equal to the sum of that of the lift nozzles, 35 mm in this case. The fuselage model is approximately 1 m in length and was mounted with the longitudinal axis horizontal to facilitate flow visualization.

The flowfield parameters were chosen to determine the sensitivity of near-field acoustics to aircraft configuration and operating conditions. The nozzles were operated at pressure ratios of 3.0, 3.5, and 4.0, corresponding to overexpanded, design point, and underexpanded conditions for the CD nozzles, respectively. The normalized distance to the ground plane, h_n/d_e, was varied from 2 to 9 based on jet-induced lift data. Unpublished force balance data shows that at $h_n/d_e = 9$ the fuselage is out of ground effect. At $h_n/d_e = 4$ and 6, entrainment effects produce strong suck-down forces. At $h_n/d_e = 2$, there is strong interaction with the ground plane that produces positive lift on the fuselage.

Near-Field Acoustic Measurements

A series of measurements to characterize the basic physical mechanisms of the twin supersonic plume acoustic interaction was conducted using the microphone configuration shown in Fig. 3. Two Bruel and Kjaer 6.35-mm microphones were mounted on floor stands in the plane of the fuselage undersurface. The primary microphone was located in the plane containing the centerlines of both nozzles, 0.6 m from the model centerline.

The microphone signals were low-pass filtered at 80 kHz, amplified, directly digitized through a high-speed Preston A/D converter, and processed on a VAXlab laboratory computer system. A fast Fourier transform (FFT) algorithm and Hanning window were used to estimate the acoustic spectra. A peak detection and tracking algorithm was used to identify and follow the screech peaks as a function of NPR and nozzle height. For this purpose, a spectral peak is defined as an isolated spike in the spectrum that exceeds 120 dB in amplitude. Peaks below this amplitude threshold were generally indistinguishable from the background spectrum. In this section, the dependence of screech amplitude and frequency on nozzle shape and height above the ground plane is discussed.

The wavelength and amplitude of screech for the coupled twin plumes are plotted in normalized form as a function of the fully expanded jet Mach number in Figs. 4 and 5. These data were obtained using the centerline microphone for twin nozzles and a simulated fuselage, but without a ground plane.

For the axisymmetric nozzles (Fig. 4), the CT nozzles produce higher sound pressure levels (SPL) than the CD nozzles, as might be expected because the plumes of the CD nozzles are nominally shock free at the design Mach number. A mode switch (B mode to C mode) occurs for the CT nozzles at a jet Mach number of approximately 1.35, with lower SPL in the transition range between modes. When the B-mode instability is present, the amplitude of the screech frequency harmonic (denoted 2B) is greater than that of the fundamental. High-amplitude screech harmonics have also been observed by Seiner et al.[3] for isolated transducer locations in twin-plume coupling measurements and may be the result of a different directivity pattern for the screech fundamental and harmonic. The fundamental is dominant for the C mode, but only the

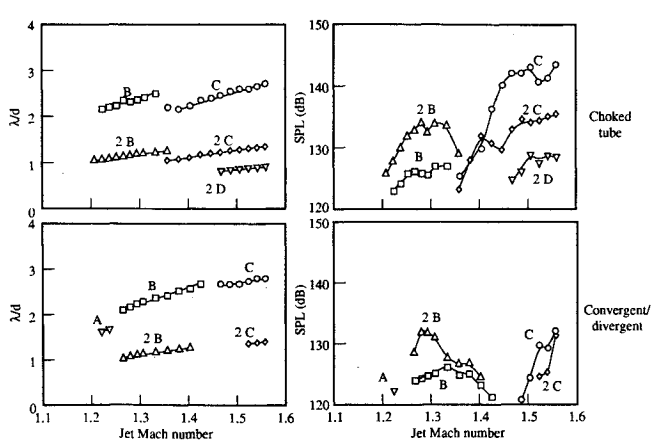

Fig. 4 Resonance modes for nonimpinging axisymmetric jets.

harmonic of the D-mode frequency is extracted using the peak-detection criterion described earlier.

The round CD nozzle has similar screech frequency characteristics, except that the mode transition occurs near the design Mach number of the nozzle, 1.47. Screech is not detectable at the design Mach number, but is clearly present when the flow is under- or overexpanded. The decrease in screech amplitude is consistent with data for isolated CD nozzles.[11] In previous studies, screech coupling existed at the design Mach number of the nozzles even at the widest nozzle spacing ($s/d = 3.2$), and in other studies, plume coupling was shown to persist to $s/d = 10$ (Ref. 12). However, results for convergent nozzles[14] indicate that plume coupling decreases sharply for $s/d > 4$. In the present study ($s/d = 4.16$), the nozzles may be spaced sufficiently far apart to suppress plume coupling at the design Mach number of the nozzles.

For the 2:1 rectangular nozzles (Fig. 5), the fundamental mode is strongest at all Mach numbers. Since no naming convention has been established for the rectangular plume screech modes, the designations R1 and R2 are used in the figures. Evidence of the screech fundamental along the fuselage centerline is indicative of a symmetric plume interaction mode, where the term interaction mode pertains to the relative phase relationship between two plumes in screech.[13] Antiphase coupling would produce destructive interference at the fundamental frequency along the fuselage centerline. Flow visualization results discussed in the following show that the plume interaction mode is of the lateral symmetric (LS) type, using the naming convention of Ref. 13.

A second set of data was obtained to determine the variation of screech and impingement amplitude and frequency with distance from the ground plane for the various nozzle

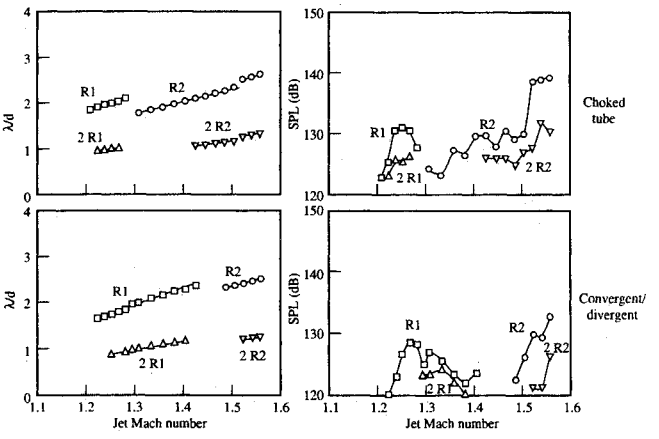

Fig. 5 Resonance modes for nonimpinging rectangular jets.

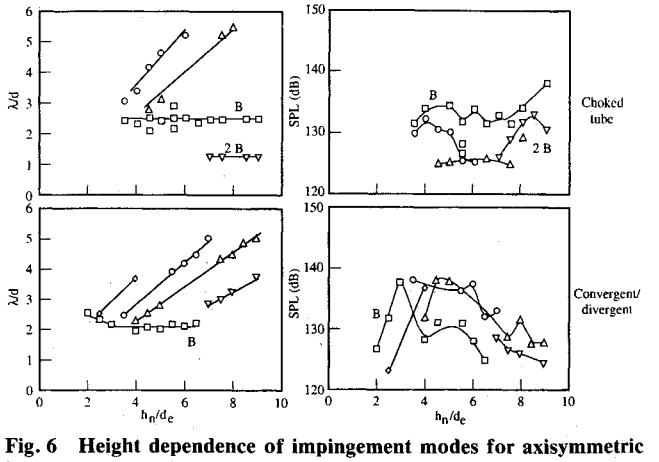

Fig. 6 Height dependence of impingement modes for axisymmetric jets.

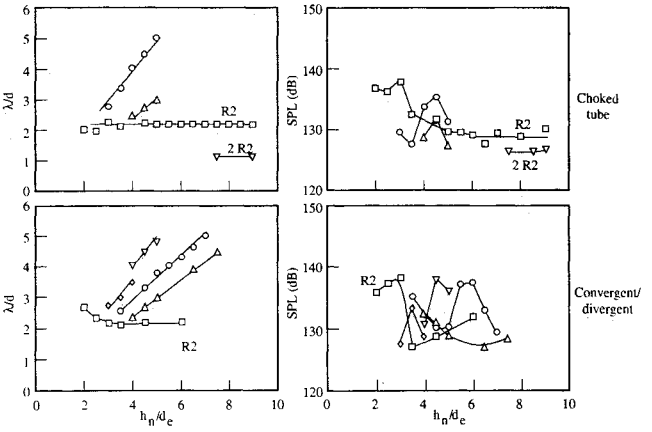

Fig. 7 Height dependence of impingement modes for rectangular jets.

configurations (Figs. 6 and 7). The nozzles were operated at NPR = 3.5, the design NPR for the CD nozzles. In this case, pure tones observed in the spectra could either be screech or impingement tones. When the normalized wavelength is plotted as a function of height above the ground plane, screech is characterized by horizontal lines because the screech frequency is generally insensitive to distance from the ground plane. The impingement tones appear as a series of diagonal lines because the resonant wavelength is linearly related to distance from the nozzles to the ground plane. Changes in the slope of the diagonals are characteristic of impingement tone staging, as observed by Norum[6] for single impinging supersonic plumes.

For the axisymmetric CT nozzles (Fig. 6), plume screech is the dominant noise source for $h_n/d_e > 3$. Below that point, no resonance peaks are observed, probably because the total amplification of the shear-layer instability waves between the nozzle and the plate is insufficient to sustain self-excited oscillation. The other tones present show some evidence of staging, but the impingement tone amplitudes are always lower than those due to screech. Thus, the presence of a strong screech resonance appears to interfere with the development of impingement modes.

A discrete screech peak is not present for the CD nozzles at the design NPR = 3.5 when $h_n/d_e > 7$, which is consistent with the data of Fig. 4. The screech tone manifests itself only as the distance to the ground plane is decreased, probably because distortion of the entrainment flow due to proximity to the ground plane produces shocks in the plume. There is evidence of strong impingement tones and tone staging at all heights above the ground plane, and the impingement tones have amplitudes greater than the screech amplitude except for locations very close to the ground plane.

A comparison between the CT and CD data for $h_n/d_e < 6$ leads to the rather remarkable conclusion that the CD nozzles operating at their design point produce more intense impingement tones than the underexpanded plumes from the CT nozzles. The flowfield characteristics are such that high-amplitude screech resonance tends to occur when impingement tones are weak. Furthermore, when screech is suppressed by using the CD nozzles at their design pressure ratio, strong impingement tones produce greater overall acoustic levels for all $h_n/d_e < 6$.

The data for the rectangular nozzles (Fig. 7) show similar trends to those of the axisymmetric nozzles. The rectangular nozzles tend to produce greater acoustic levels than the axisymmetric nozzles for $h_n/d_e < 4$, but the amplitudes decrease rapidly with increasing distance from the ground plane. Suppression of impingement tones is observed when strong screech is present. The rectangular CD nozzles produce strong impingement tones and greater overall acoustic levels than

their choked-tube counterparts for $4 < h_n/d_e < 7$. It should be noted that these conclusions are based on a single centerline microphone location; the surface acoustic load data discussed in the following show that impingement tone suppression leads to a reduction in overall unsteady surface pressures.

Flow Visualization

A shadowgraph system aligned along the centerline was used to visualize plume oscillation in a plane normal to the fuselage centerline. The flow was imaged through two 400-mm mirrors using a video camera and a high-quality video recording system. A strobe light focused through a pinhole and synchronized to the video system was used as the light source. The same centerline microphone was used for phase conditioning.

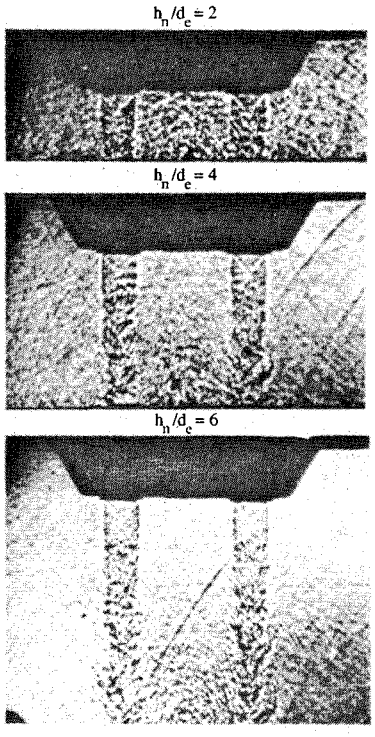

Fig. 8 Phase-locked shadowgraph visualization of impinging axisymmetric jets; CD nozzles; NPR = 4.0.

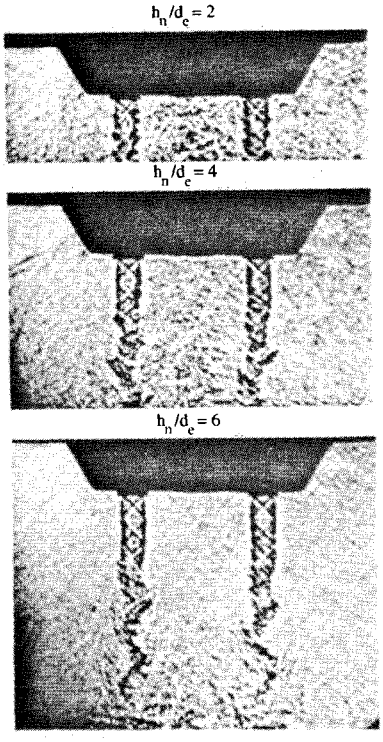

Fig. 9 Phase-locked shadowgraph visualization of impinging rectangular jets; CD nozzles; NPR = 4.0.

Typical shadowgraph images for the axisymmetric CD nozzle operating at the off-design pressure ratio of 4.0 and phase locked to the strongest resonance tones are shown in Fig. 8. There is little evidence of the screech and impingement instabilities in these images. This is in sharp contrast to the 2:1 nozzles (Fig. 9), which show highly ordered periodicity for $h_n/d_e > 2$ for which large acoustic amplitudes have been measured. An isolated 2:1 plume oscillates normal to the major axis of the nozzle; thus, two plumes aligned with their major axes parallel tend to couple and produce high acoustic amplitudes. Flow visualization movies for these configurations show that the plumes are generally symmetrically phased, but occasionally flip to antiphase synchronization when perturbed by the fountain upwash. For $h_n/d_e = 2$, small-scale shear-layer instabilities are observed in the plumes, but there is insufficient axial distance for the large-scale plume instability to develop.

A shadowgraph is of limited utility for visualizing the fountain flowfield because of the weak gradients in the fountain upwash. A laser-sheet visualization system (Fig. 10) was used to illuminate selected cross sections of a flow seeded with a water mist. A thin laser sheet was generated normal to the centerline of the model. The field of view is essentially the same as that of the shadowgraph system, but the laser sheet illuminates selected planes within the flowfield. A 20-W Cu vapor laser is focused into a slowly converging/diverging sheet that has minimum thickness at the model. The laser pulses at

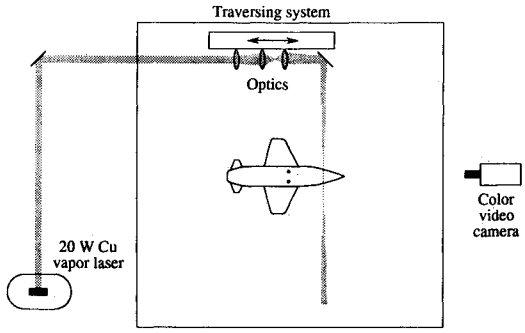

Fig. 10 Laser-sheet flow visualization configuration.

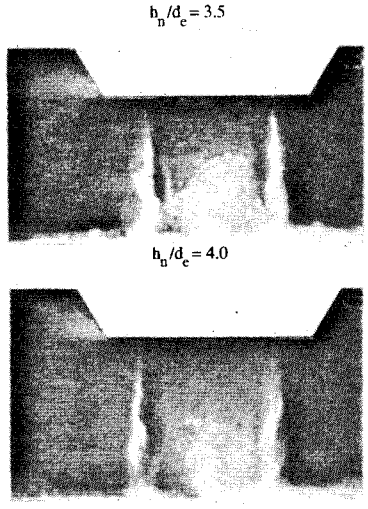

Fig. 11 Phase-locked laser-sheet visualization of impinging rectangular jets; CD nozzles; NPR = 4.0.

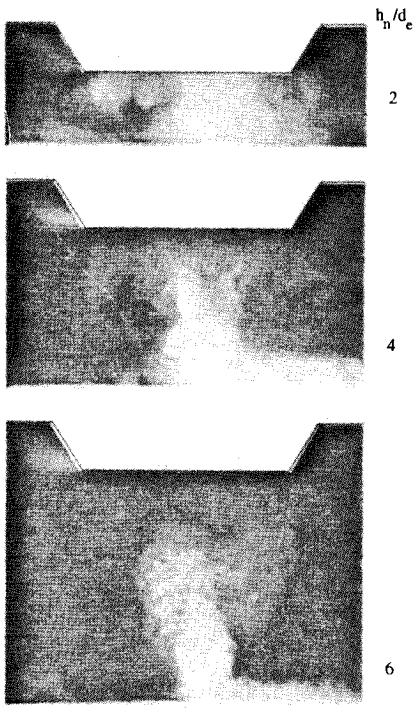

Fig. 12 Laser-sheet visualization of upwash fountain; axisymmetric CD nozzles; NPR = 4.0.

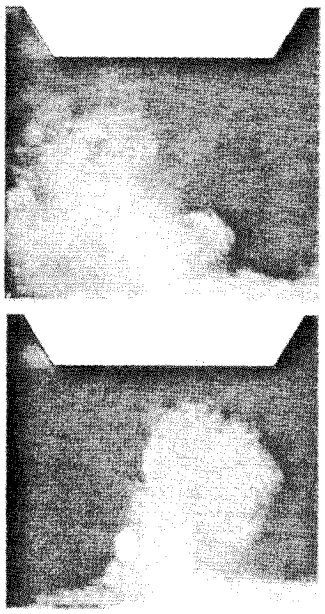

Fig. 13 Laser-sheet visualization of bistable fountain; axisymmetric CD nozzles; NPR = 4.0; $h_n/d_e = 6$.

a free-running frequency of 10 kHz, but can also be phase locked to periodicities in the flow in cases where the flow is highly periodic.

An electronically shuttered color video camera is used to image the flow. The electronic shutter opens for a span of 0.5 ms; thus, each frame of the video is an average over five pulses of the laser system. The sheet-forming optics are mounted on a single-axis traverse that permits visualization of selected planes from the nose of the model to the aft of the nozzles. Thus, the plumes and the upwash fountain can be selectively made visible.

The 2:1 rectangular nozzles were the only configuration that produced sufficiently regular impingement tones to permit phase synchronization with the Cu vapor laser. The signal from the centerline microphone was filtered at the screech frequency and converted to a square-wave trigger at approximately 2 kHz. Examples of the phase-locked visualization are shown in Fig. 11. In this case, the laser sheet is positioned through the centerline of the nozzles. The water mist is concentrated in the outer edges of the plumes, thereby emphasizing the shear-layer structure rather than the plume core flow. At $h_n/d_e = 3.5$, the plumes are nearly antiphase, whereas at $h_n/d_e = 4.0$, the symmetric plume coupling is evident.

Examples of fountain visualization that are not phase locked to the plume instabilities are shown in Figs. 12 and 13. Although these images were obtained for the axisymmetric CD nozzles, there was no discernible difference in the upwash characteristics among all of the nozzle configurations. The laser sheet is located forward of the plane of the nozzles to de-emphasize the plumes and to make the fountain upwash visible. At $h_n/d_e = 2$ (Fig. 12), a pair of counter-rotating vortices form under the fuselage and along the axis of the aircraft to produce a stable upwash flow. For $h_n/d_e = 4$ and 6, the fountain is less stable and more asymmetric.

In most cases for $h_n/d_e > 3$, the fountain becomes bistable (Fig. 13). Instead of impinging along the centerline of the fuselage, the fountain is deflected toward one plume in a quasistable orientation. At random intervals, the plume flips to the opposite side of the model axis. The wandering of the fountain has a relatively long time scale in comparison with that of the jet flow, e.g., on the order of seconds for the model scale configuration. Some fountain upwash is entrained directly into one of the plumes, potentially reducing the hydrodynamic loading from fountain impingement on the fuselage.

Undersurface Dynamic Pressure Measurements

The array of 40 Kulite pressure transducers used for the surface dynamic loads measurements is shown in Fig. 2. Cylindrical transducers were mounted in holes in the fuselage, and flat-pack transducers were mounted to the wing undersurfaces. The transducers were rated at 50 psi full scale because of the anticipated large mean loads due to fountain impingement. Accurate estimates of the transducer acoustic loads were obtained by high-pass filtering the raw signals, providing sufficient gain to drive the data acquisition A/D converters, and by regular piston-phone calibrations. The transducers were arranged in a pattern concentrated along the fuselage centerline near the nozzles, taking advantage of the bilateral symmetry of the model. Three additional transducers were added to the opposite side of the model centerline as a symmetry check.

The pressure transducers were subdivided into banks of 11, with the centerline microphone connected to channel 12 of each bank. A switching system was used to couple the raw signals to a 12-channel data acquisition system. The raw signals were AC coupled and low-pass filtered at 40 kHz by a 12-channel Wavetek Brickwall antialiasing filter system. Manually controlled gain was applied to each channel before digitization. The data were acquired at 80 kHz per channel by a Preston A/D converter driven by a VAXlab computer system.

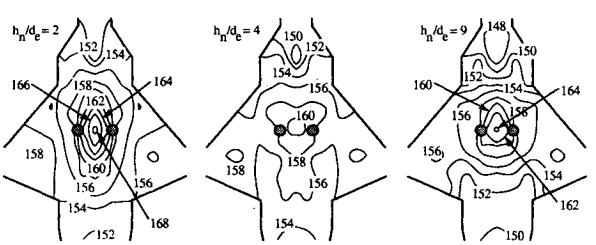

Fig. 14 Undersurface dynamic pressure distributions for axisymmetric choked-tube nozzles; NPR = 3.5.

The VAXlab system continuously monitored input levels and specified gain changes to maximize the input signal levels.

After digitization, the spectrum was computed for each transducer using an on-line FFT algorithm. The phase and coherence relative to the reference microphone were also determined to distinguish between symmetric and antisymmetric plume interaction modes. The overall sound pressure levels (OASPL) were computed by direct integration of the spectra.

The data presented in this paper are limited to maps of OASPL. Contour plots of the undersurface loading were generated by interpolating the pressure sensor data onto a regular grid representing the fuselage and wings of the model undersurface.

The distribution of undersurface dynamic pressures for the CT nozzles at h_n/d_e of 2, 4, and 9 are shown in Figs. 14 and 15. For both the axisymmetric and rectangular nozzle configurations, the region of maximum dynamic loading occurs between the nozzles at $h_n/d_e = 2$. Thus, the dominant loading mechanism is neither screech nor impingement tones, but is instead the unsteady hydrodynamic loading from the upwash fountain flow directly impinging on the fuselage undersurface.

The fountain flow is turbulent and highly unsteady, as illustrated by the laser-sheet flow visualization. Therefore, pressure fluctuations of the order of several percent of the total dynamic pressure in the fountain flow might be expected. The flow visualization also shows that the fountain spreads rapidly so that the greatest dynamic loads occur when the fuselage is close to the ground plane. As the distance from the ground plane increases, the relative magnitude of the loading due to the upwash fountain tends to decrease relative to the loads on the wings and the fore and aft fuselage. This decrease is consistent with the weakening of the fountain.

The rectangular nozzles produce significantly greater unsteady loads on the fuselage for small h_n in comparison with the round nozzles. At $h_n/d_e = 2$, the 164-dB contour has a substantially larger footprint and typical wing loads are 4 to 6 dB greater than those for the round nozzles. At larger h_n, the fuselage loads are of the same order or lower than that for the other nozzles, but increase on the wing. These differences are a consequence of the strong lateral screech coupling observed for this configuration. The intense screech and impingement tones tend to increase the fuselage loading in regions away from the fountain impingement zone. The wing loading pattern is consistent with the acoustic directivity of the rectangular plume flapping mode.

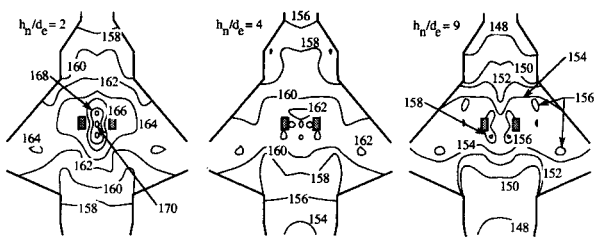

Fig. 15 Undersurface dynamic pressure distributions for rectangular choked-tube nozzles; NPR = 3.5.

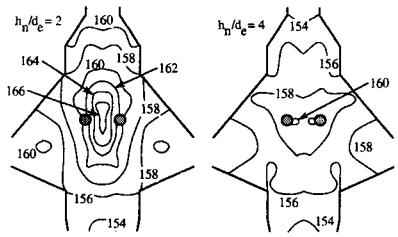

Fig. 16 Undersurface dynamic pressure distributions for rectangular CD nozzles; NPR = 3.5.

The effect of operating the axisymmetric CD nozzles at their design pressure ratio is illustrated in Fig. 16. At $h_n/d_e = 2$, the peak fuselage loads decrease slightly relative to those of the CT nozzles, but the acoustic loads generally increase over the remainder of the fuselage. The increase is probably a consequence the increased impingement tone amplitude observed in the near-field microphone data. At $h_n/d_e = 4$, the loading footprint also increases slightly. For small h_n, the impingement tones tend to be augmented for the CD nozzles. This somewhat surprising result suggests that simple convergent nozzles with slightly reduced performance may reduce unsteady loads by suppressing the plume impingement modes.

Conclusions

The nearfield acoustic environment of a model-scale STOVL aircraft has been investigated in proximity to a ground plane. Near-field microphone measurements, flow visualization, and surface dynamic pressure distributions were used to determine the primary mechanisms by which unsteady loads are developed on the aircraft undersurface. There are three primary sources of unsteady loading that vary in importance depending on the configuration parameters.

Fountain Impingement

The unsteady fountain impinges along the centerline of the fuselage and produces the greatest dynamic loads in the region between the nozzles, particularly when the fuselage is in proximity to the ground plane ($h_n/d_e = 2$). When the aircraft is out of ground effect ($h_n/d_e > 4$), the fountain loads diminish and other acoustic sources become more important. The fountain characteristics have a weak dependence on nozzle configuration, with the axisymmetric nozzles producing the largest unsteady loads on the fuselage centerline. In some cases when $h_n/d_e > 2$, the fountain meanders between two asymmetric states on either side of the fuselage centerline.

Impingement Tones

Impingement tones exist for all nozzle configurations and have a frequency variation with Mach number consistent with staging. The highest amplitudes are produced when screech is minimized using CD nozzles at their design Mach number; the OASPL in these cases are greater than for the choked-tube nozzles operating at the same conditions. The impingement tones are a dominant source of dynamic loads only in regions away from direct fountain impingement, such as the wings and fore and aft fuselage. The rectangular jets generate the greatest wing loads because of strong coupling between the plumes. Consistent with the near-field acoustic data, the axisymmetric CD jets produce slightly greater wing loads than their choked-tube counterparts.

Screech

As with the impingement tones, screech is a significant loading source only in areas outside the fountain impingement zone. There is no evidence of screech coupling for the convergent/divergent nozzles at their design pressure ratio.

In conclusion, the best strategy for dynamic load alleviation appears to be the reduction of fountain impingement loads and control of fountain unsteadiness. The rectangular nozzles are better from this standpoint, but produce larger wing loads due to the generation of intense impingement tones. Furthermore, simple nozzles without CD contours tend to reduce the overall fuselage dynamic loads by suppressing impingement tones while supporting weaker screech modes.

Acknowledgment

This research was performed under NASA Contract NAS1-18745 at the McDonnell Douglas Research Laboratories and the McDonnell Aircraft Company.

References

[1]VanOverbeke, T. J., and Holdeman, J. D., "A Numerical Study of the Hot Gas Environment Around a STOVL Aircraft in Ground Proximity," AIAA Paper 88-2882, July 1988.

[2]Seiner, J. M., Manning, J. C., and Ponton, M. K., "Dynamic Pressure Loads Associated with Twin Supersonic Plume Resonance," *AIAA Journal*, Vol. 26, No. 8, 1988, pp. 954–960.

[3]Seiner, J. M., Ponton, M. K., Pendergraft, O. C., Manning, J. C., and Mason, M. L., "External Nozzle Flap Dynamic Load Measurements on F-15 S/MTD Model," AIAA Paper 90-1910, July 1990.

[4]Krothapalli, A., "Discrete Tonjes Generated by an Impinging Underexpanded Rectangular Jet," *AIAA Journal*, Vol. 23, No. 12, 1985, pp. 1910–1915.

[5]Ahuja, K. K., and Spencer, D. A., "Aeroacoustics of Advanced STOVL Aircraft Plumes," *Proceedings of the International Powered Lift Conference*, SAE, (Santa Clara, CA), Dec. 1987, pp. 531–541.

[6]Norum, T. D., "Supersonic Rectangular Jet Impingement Noise Experiments," AIAA Paper 89-1138, April 1989.

[7]Saripalli, K. R., "Laser-Doppler Velocimeter Measurements in a Three-Dimensional Impinging Twin-Jet Fountain Flow," AIAA Paper 85-4036, Oct. 1985.

[8]Kibens, V., Saripalli, K. R., Wlezien, R. W., and Kegelman, J. T., "Unsteady Features of Jets in Lift and Cruise Modes for VTOL Aircraft," *Proceedings of the International Powered Lift Conference*, SAE (Santa Clara, CA) Dec. 1987, pp. 543–552.

[9]Childs, R. E., and Nixon, D., "Unsteady Three-Dimensional Simulations of a VTOL Upwash Fountain," AIAA Paper 86-0212, Jan. 1986.

[10]Childs, R. E., Nixon, D., Kuhn, G. D., and Perkins, S. C., "Further Studies of Impinging Jet Phenomena," AIAA Paper 87-0017, Jan. 1987.

[11]Wlezien, R. W., "Nozzle Geometry Effects on Supersonic Jet Interaction," *AIAA Journal*, Vol. 27, No. 10, 1989, pp. 1361–1369.

[12]Shaw, L., "Twin Jet Screech Suppression," AIAA Paper 89-1140, April 1989.

[13]Zilz, D. E., and Wlezien, R. W., "The Sensitivity of Near-Field Acoustics to the Orientation of Twin Two-Dimensional Supersonic Nozzles," AIAA Paper 90-2149, July 1990.

[14]Walker, S., "Twin Jet Screech Suppression Concepts Tested for 4.7% Axisymmetric and Two-Dimensional Nozzle Configurations," AIAA Paper 90-2150, July 1990.